

VHF meteor radar at King Sejong Station, Antarctica

Jeong-Han Kim^{1*}, Geonhwa Jee¹, Changsup Lee^{1,2} & Yong-Ha Kim²

¹Division of Polar Climate Research, Korea Polar Research Institute, 26 Songdomirae-ro, Incheon 406-840, Korea;

²Department of Astronomy and Space Science, Chungnam National University, 79 Daehangno, Yuseong-gu, Daejeon 305-764, Korea

Received 9 July 2013; accepted 25 November 2013

Abstract Since 2002, we have been observing the mesosphere and lower thermosphere (MLT) region over King Sejong Station (KSS; 62.22°S, 58.78°W), Antarctica, using various instruments such as the Spectral Airglow Temperature Imager (SATI), All Sky Camera (ASC) and VHF meteor radar. The meteor radar, installed in March 2007, continuously measures neutral winds in the altitude region 70–110 km and neutral temperature near the mesopause 24 h⁻¹, regardless of weather conditions. In this study, we present results of an analysis of the neutral wind data for gravity wave activity over the tip of the Antarctic Peninsula, where such activity is known to be very high. Also presented is temperature estimation from measurement of the decay times of meteor trails, which is compared with other temperature measurements from SATI and the Sounding of the Atmosphere using Broadband Emission Radiometry (SABER) instrument onboard the Thermosphere Ionosphere Mesosphere Energy and Dynamics (TIMED) satellite.

Keywords meteor radar, gravity wave, mesosphere and lower thermosphere region, Antarctica

Citation: Kim J H, Jee G, Lee C, et al. VHF meteor radar at King Sejong Station, Antarctica. *Adv Polar Sci*, 2013, 24:241-247, doi: 10.3724/SP.J.1085.2013.00241

1 Introduction

Atmospheric waves such as gravity waves (GW), planetary waves and tides, which mostly propagate from the lower to upper atmosphere, are very important factors in determining the dynamics and energetics of the mesosphere and lower thermosphere (MLT) region. Such waves have been extensively studied over several decades^[1-2]. A VHF meteor radar has been operated since March 2007 at King Sejong Station (KSS; 62.22°S, 58.78°W), Antarctica for observations of the MLT region. Although satellite observations have become a major contributor to current studies of the upper atmosphere, ground-based observations remain important, particularly in the polar region where satellite observations are limited. Meteor radar has been extensively used as a very useful tool to investigate atmospheric wave activities in the MLT region^[3-5]. Meteor radar observations not only provide neutral winds, but also allow estimation of neutral temperatures near the

mesopause region from measured decay times of meteor trails. A number of studies were devoted to determining atmospheric temperature from the relationship between the temperature and diffusion coefficient of the decay of meteor trails, which can be calculated from measurements of meteor decay times under the assumption of ambipolar diffusion of ions and electrons within meteor trails^[6-14].

In this work, we summarize results of recent studies of the MLT region using data from the VHF meteor radar at KSS, near the tip of the Antarctic Peninsula. This region is often exposed to the boundary of the Antarctic winter stratospheric vortex, where GW activity is known to be very high^[15]. In the subsequent sections, a brief introduction to the meteor radar system is given, followed by a summary of studies on GW activity and temperature estimation from the meteor radar measurements.

2 VHF meteor radar

Unlike optical instruments that only operate on moonless clear nights, radar instruments are relatively immune to weather conditions and can be operated continuously day

* Corresponding author (email: jhkim@kopri.re.kr)

and night and year round. In addition to existing optical observations for the MLT region at KSS in Antarctica, a VHF meteor radar system was installed in March 2007 for studying upper atmospheric dynamics and temperature variation near the mesopause region^[13-14,16]. The radar supplied by ATRAD Pty Ltd. is an interferometric radar consisting of a cross-folded dipole transmitting antenna and five receiving antennas along two perpendicular directions, with spacings of 2λ and 2.5λ to minimize mutual antenna coupling. The radar operates at 33.2 MHz, with peak power 8 kW and maximum duty cycle 8.4% to receive meteor echoes reflected from underdense meteor trails. Operational parameters of the KSS meteor radar are summarized in Table 1. Radar details are described in Holdsworth et al.^[17-18].

Table 1 Operating parameters for meteor observations using King Sejong Station meteor radar

Parameter	Value
Frequency/MHz	33.2
Frequency agility/kHz	± 100
Transmit power/kW	8
Transmit polarization	Circular
EPW/($m \cdot \mu s^{-1}$)	7 200/47.95
PRF/Hz	440
Duty cycle/%	8.4%
Receiver-filter width/kHz	18.1
Pulse code type	4-bit complementary
Pulse shape	Gaussian
Range/km	80–307
Range sampling resolution/km	1.8
Coherent integrations	4
Effective sampling time/s	0.009
Number of samples	12 650
Acquisition length/s	115

The all-sky interferometric meteor radar collects meteor echoes over the full range of zenith angle, but the data used here were restricted to between 10° and 75° to remove unnecessary data uncertainties. Meteor echoes at large zenith angles are reflected from near the horizon and may contain significant atmospheric effects owing to, for example, water vapor, ions and electrons along the signal path, which may cause errors in range determination. Echoes at small zenith angles, on the other hand, are reflected from near the zenithal direction, so have small radial velocities. This may cause large errors in the determination of horizontal wind. To ensure unambiguous detection of meteors, the data were limited to signal-to-noise ratios about 7.4 dB or greater.

The radar system has been run continuously from March 2007 until the present. Data collected during March 2007 through October 2009 were used to investigate meteor decay time behavior^[13,16], mesospheric temperature estima-

tion using meteor decay times^[14], and seasonal variations of GW activity (Lee et al., submitted). These investigations are summarized in the following sections.

3 Seasonal variations of gravity wave activity inferred from neutral wind data

The variance of horizontal wind velocities measured by meteor radar has been generally used as a proxy for the activity of small-scale GWs^[3,19]. The simple wind variance technique uses the difference between hourly average winds of a height-time sector and estimated horizontal winds from radial velocities of individual meteor echoes within the sector. In this study, we used a simple assumption in which large-scale atmospheric motions in the meteor observation region, which has a ~ 250 -km radius, are homogeneous and remain constant within a relatively short time interval (~ 1 h). Once we removed the contribution of large-scale motions such as mean winds and tides, resulting variances of horizontal winds were assumed due to small-scale GWs. These variances were used to study GW characteristics over KSS with horizontal wavelengths up to 400 km and periods less than ~ 3 h, between 82- and 98-km altitudes.

To investigate seasonal variations of small-scale GW activity, monthly means of wind variances were calculated (Figure 1). In most seasons, the variances increased with height, except for November and December, which had decreasing trends with height below about 90 km. Clear seasonal variation is seen in both zonal and meridional wind variances, with higher-altitude maxima in May and around September. In particular, as with tidal amplitude (not shown), there were sudden and large enhancements in May, which may indicate that GW activity suddenly increased in the lower atmosphere around May near KSS. It is known that there is formation and breakdown of the Antarctic vortex in the lower atmosphere (upper troposphere through stratosphere) in autumn and spring, respectively, which may partially contribute to the enhancement of GW activity^[20].

The consistent seasonal variations between semidiurnal tides and GW activities may indicate tidal modulation of those activities. However, height profiles of the wind variances showed significantly different behaviors in summer (November and December). In general, GWs can propagate upward with slower phase velocities and they are strongly affected by the background wind (primarily the zonal wind), unlike tides^[21]. The strong westward wind below 80-km altitude during summer may cause the GW amplitudes to break rapidly as they propagate through the background wind (Figure 1).

Although the seasonal and height dependences of wind variances are consistent with previous studies of various southern high latitude regions, the wind variances over KSS seem particularly large compared with other regions. For example, the variances are larger than those observed at Rothera Station in the mid Antarctic Peninsula (Figure 6 in

[19]). In particular, this difference becomes significant above 88 km, with a ratio as large as ~ 1.5 at 98 km during the winter season. These discrepancies imply that the generation and propagation of GWs can be significantly affected by spatially localized sources and background environments, such as local GW breaking and wind fields^[22]. Baumgaertner and McDonald^[15] and Whiteway et al.^[23] reported strong enhancement of wave energy at the bound-

ary of the polar vortex and concluded that the large zonal winds near the polar vortex lead to Doppler shift of the vertical wavelength of GWs with relatively small phase velocity toward larger wavelengths. Such large vertical wavelengths would allow GWs to propagate to higher altitude with enhanced amplitudes, prior to reaching the level of instability and breaking to deposit their energy and momentum to the background atmosphere.

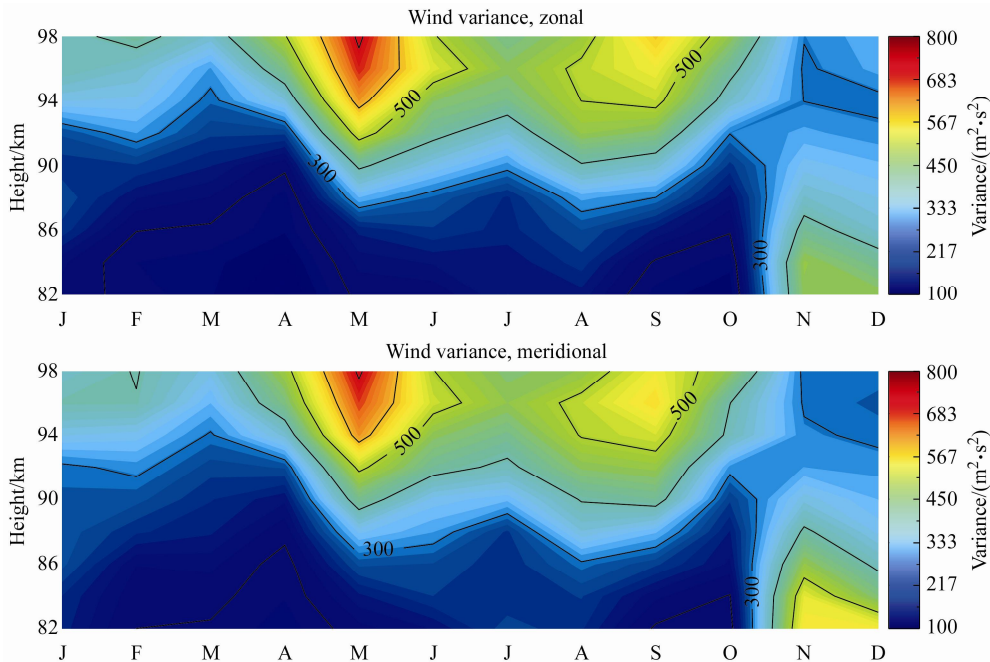


Figure 1 Height-month contour plots of monthly mean of median zonal (top) and meridional (bottom) wind variances.

4 Mesospheric temperature estimation

4.1 Seasonal variations of meteor decay times

Defined as the time over which the amplitudes of reflected signals fall to one half the maximum amplitude, meteor decay times are closely related to atmospheric temperature and pressure. A number of studies have been dedicated to estimation of mesospheric temperature using measurements of meteor decay times and their relationship to the temperature^[24-25]. As a preliminary study of temperature estimation, measurements of meteor decay time were analyzed to investigate its seasonal variation and the relationship with plasma density strength within meteor trails^[13].

It is well known that according to the ambipolar diffusion theory, meteor decay time and atmospheric density both decrease with altitude. However, recent studies have reported that the behavior of meteor decay times shows the opposite behavior below about 85 km altitude^[24-26]. The studies also showed that altitude variations of meteor decay time were dependent on the strength of plasma line density within meteor trails. The varying behavior of meteor decay times at lower altitude may be related to the occurrence of ice particles, which causes noctilucent cloud (NLC) near

the coldest summer mesopause in the polar region^[24,26]. However, Kim et al.^[13] stated that this behavior appears to persist through all seasons, although the turning altitude from the ambipolar diffusion varies with season, as clearly shown in Figure 2. This figure shows height profiles of the observed decay times for four different seasonal cases: January 2009, April 2007, July 2009, and October 2008. The dashed curves are model decay times, with upper (left curve) and lower (right curve) limits of electron density. The dash-dot line in the top left panel represents the diffusion-only model (see reference [13] for details). Using a simple model decay time with an empirical recombination rate of electrons in the D-region, they also showed that the height profile of decay times was significantly dependent on strength of the estimated relative electron line density along the meteor trail^[13,24]. This characteristic is presented in the left and right columns of Figure 2, with low (weak) and high (strong) electron line densities in meteor trails, respectively. In this figure, it is clear that the model profiles are nearly the same as the diffusion-only model between ~ 85 –95 km above the peak altitude, and are in good agreement with observed decay times for weak meteors. On the other hand, those decay times for strong meteors are strongly divergent from the diffusion-only model above the peak altitude, and are also significantly different from the

model profile over the entire altitude range.

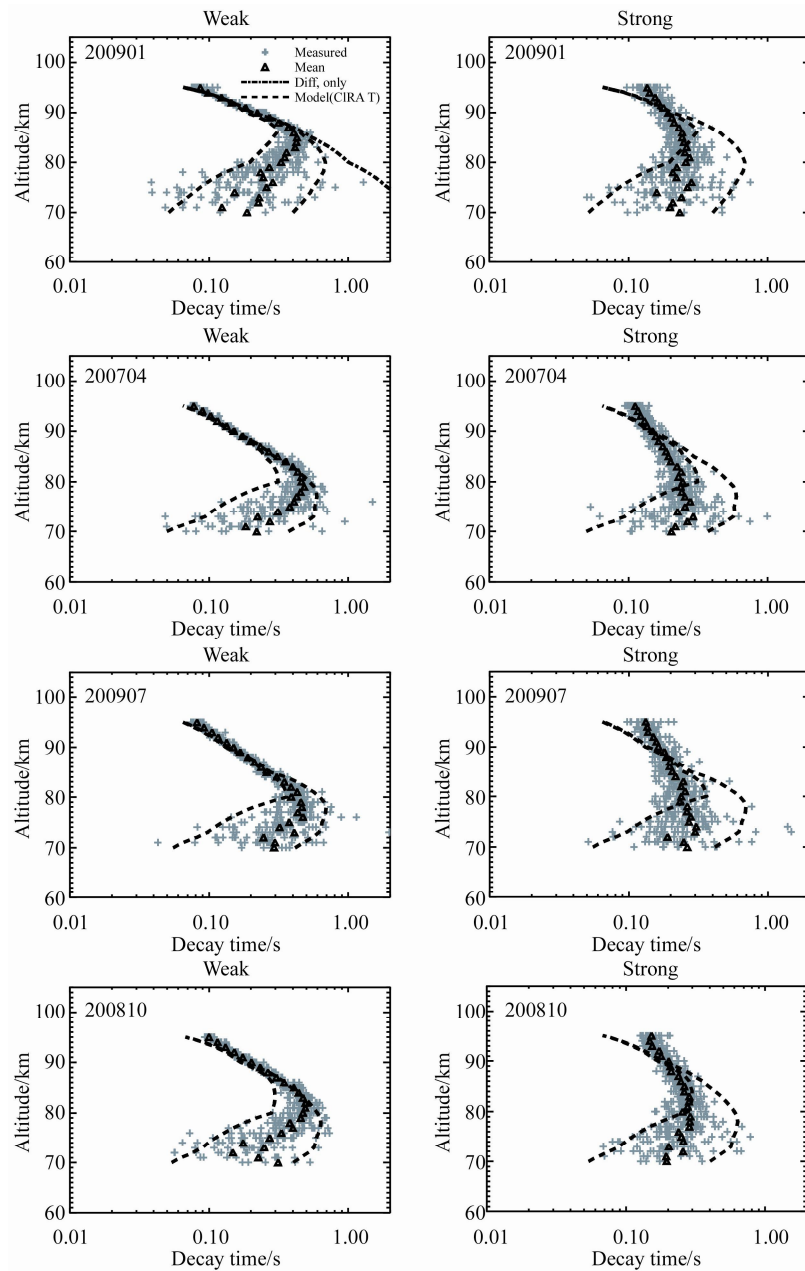


Figure 2 Height profiles of observed meteor decay times (light plus signs and dark triangles). Model decay times are overlapped with dashed lines for January, April, July, and October. The long and short model decay time profiles are for computed electron densities $2.5 \times 10^5 \text{ cm}^{-3}$ and $2.2 \times 10^6 \text{ cm}^{-3}$ in the meteor trails, respectively. A diffusion-only model is shown by a dash-dot line for the January weak meteor case^[13].

The decreasing trend in the region below the peak altitudes cannot be explained by ambipolar diffusion; additional processes are involved. By adopting the empirical recombination in the decay time model of Friedrich et al.^[27], Kim et al.^[13] were able to reproduce the decreasing trend of meteor decay times for all seasons. More recently, using numerical simulations with data from the KSS meteor radar and Aura/MLS instrument, Lee et al.^[16] pointed out that the turning altitude is a function of the background neutral density and initial electron line density of the trail. Furthermore,

they concluded that three-body attachment of meteor trail electrons to neutral atmospheric molecules is responsible for deionization of meteor trails at low altitudes and attendant turnaround of the decay-time height profile^[16].

4.2 Temperature estimation from meteor decay times

The diffusion coefficient of meteor trails, which can be determined from meteor decay times, is closely related to atmospheric temperature and pressure. With the measure-

ments of meteor decay times, atmospheric temperature can be estimated from the following equation developed by Hocking^[8]:

$$T = S \left(2T_g + \frac{mg}{k} \right) \log_{10} e, \quad (1)$$

where k is the Boltzmann constant, g is the gravitational constant at meteor peak height, m is the mass of typical atmospheric molecules, S is slope of the scatter plot of $\log_{10}(1/\tau_{1/2})$ versus height, and T_g is the temperature gradient at meteor peak altitude. The last two variables must be determined for the temperature estimation. The slope can be determined from a scatter plot of the logarithmic inverse decay times versus height (Figure 3).

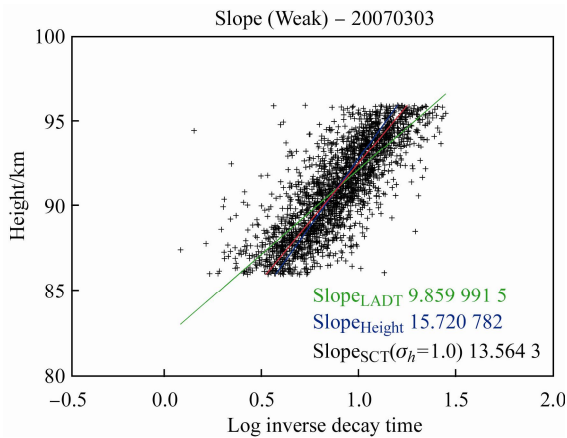


Figure 3 Scatterplot of log inverse decay time as a function of height for the weak meteor group measured on 3 March 2007. The green, blue, and red solid lines indicate linear fits using d and h as the independent variables, and linear fit using SCT method for height with σ_h of 1.0, respectively.

The optimum of the three slopes in the figure was determined by the Statistical Comparison Technique (SCT) originally developed by Hocking et al.^[28], for ascertaining the slope with a correction factor to consider errors in measurements of both height and decay time. Please refer to Kim et al.^[14] for the detailed procedure.

The secondary factor required in Eq. (1) is the temperature gradient at meteor peak height, where the determination of slope is most weighted. Kim et al.^[14] developed a temperature gradient model, by averaging temperatures obtained from Sounding of the Atmosphere using Broadband Emission Radiometry instrument onboard the Thermosphere Ionosphere Mesosphere Energy and Dynamics (TIMED) satellite TIMED/SABER between 86–96 km height during 2003–2009 over the location of KSS. However, this satellite observation record has missing periods over this location, owing to the SABER yaw cycle. The record was therefore supplemented by the temperature gradient model presented by Holdsworth et al.^[11] for Davis Station, Antarctica (68.6°S, 78.0°E), which is at a latitude similar to KSS (62.22°S, 58.78°W). The resulting temperature gradient model is presented in Figure 4, with SABER

(triangles) and Davis (crosses) temperature gradients.

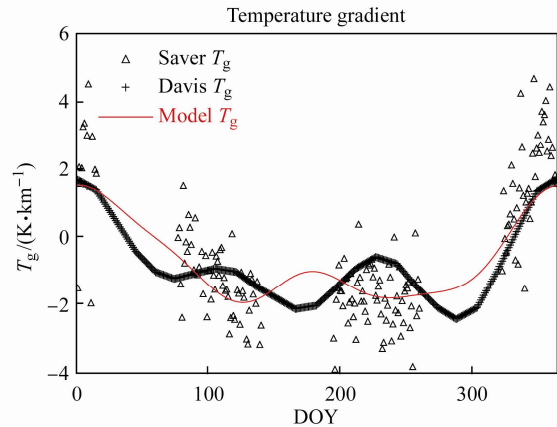


Figure 4 Model of vertical temperature gradient (red) around 91 km for the location of King Sejong Station (62°S, 59°W). The model is the result of harmonic fit with annual, semiannual, and terannual components, using daily mean SABER temperature gradient at 91 km (triangles) and Holdsworth et al. temperature gradient model (crosses)^[11].

With the determined slope and temperature gradient model, temperature was estimated from decay times of weak meteors. Figure 5a shows daily meteor temperatures during March 2007 through November 2009. Monthly SABER temperatures during 2007 through 2009 and Spectral Airglow Temperature Imager (SATI) OH and O₂ rotational temperatures during 2007 are superimposed, with diamond, square and triangle symbols, respectively. The seasonal variation of meteor temperatures is consistent with previous studies that investigated mesospheric temperature estimation from meteor decay times at various sites in the northern and southern hemispheres^[10–11,29–31].

For improved comparison of the estimated temperature with observations from SABER and SATI instruments, the monthly mean meteor temperatures were computed (Figure 5b). The meteor temperatures appear generally consistent with SABER monthly mean temperatures except for July, which shows the largest difference. This discrepancy is probably related to several meteor showers in the Southern Hemisphere in that month.

5 Conclusion

The meteor radar at KSS has provided valuable data for study of the MLT region and coupling to the lower atmosphere. To extend the data applications and compare with other measurements at KSS, accuracy of the estimated temperature must be enhanced. This can be achieved by further improvements of the temperature gradient model and the slope of logarithmic inverse decay time versus height. The resulting radar temperature will be compared with the SATI temperature obtained at the same site, as well as with satellite measurements.

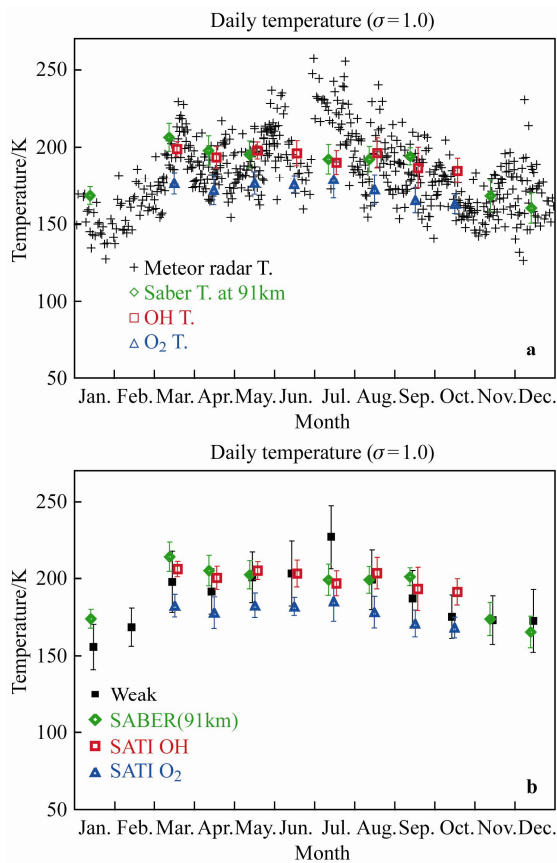


Figure 5 Daily (a) and monthly mean (b) temperatures estimated from decay times of the weak meteor group, using the temperature gradient model and height-independent slope applying σ_h of 1.0 km. SABER temperatures around 91 km and SATI OH and O₂ rotational temperatures are superimposed with green, red, and blue colors, respectively.

Other ongoing work is GW activity over KSS and the effects of atmospheric waves on the MLT region. It is known that atmospheric waves such as GW, tidal, and planetary waves propagating from the lower to upper atmosphere cause variations of dynamical and thermal states of the upper atmosphere, via dissipation of the waves. Recent studies have reported that the activities of the GWs are strong around the tip of the Antarctic Peninsula, where KSS is located^[15,32]. For improved understanding of GW effects on the MLT region over KSS, we will continue to collect data there from the meteor radar, SATI and an All Sky Camera (ASC). We will carefully analyze those data, via comparisons with observations from satellites and ground-based instruments, as well as with numerical model results.

Acknowledgements This work was financially supported by research funds (Grant nos. PE13010 and PP12320) from the Korea Polar Research Institute.

References

- 1 Holton J R. The influence of gravity wave breaking on the general circ-

- ulation of the middle atmosphere. *J Atmos Sci*, 1983, 40(10): 2497-2507.
- 2 Fritts D C, Alexander M J. Gravity wave dynamics and effects in the middle atmosphere. *Rev Geophys*, 2003, 41(1), doi: 10.1029/2001RG000106.
- 3 Dowdy A J, Vincent R A, Tsutsumi M, et al. Polar mesosphere and lower thermosphere dynamics: 1. Mean wind and gravity wave climatologies. *J Geophys Res*, 2007, 112(D17104), doi: 10.1029/2006JD008126.
- 4 Beldon C L, Mitchell N J. Gravity waves in the mesopause region observed by meteor radar, 2: Climatologies of gravity waves in the Antarctic and Arctic. *J Atmos Sol-Terr Phys*, 2009, 71(8-9): 875-884.
- 5 Placke M, Stober G, Jacobi C. Gravity wave momentum fluxes in the MLT-Part I: Seasonal variation at Collm (51.31°N, 13.01°E). *J Atmos Sol-Terr Phys*, 2010, 73(9): 904-910.
- 6 Chilson P B, Czechowsky P, Schmidt G. A comparison of ambipolar diffusion coefficients in meteor trains using VHF radar and UV lidar. *Geophys Res Lett*, 1996, 23(20): 2745-2748.
- 7 Hocking W K, Thayaparan T, Jones J. Meteor decay times and their use in determining a diagnostic mesospheric temperature-pressure parameter: methodology and one year of data. *Geophys Res Lett*, 1997, 24(23): 2977-2980.
- 8 Hocking W K. Temperatures using radar-meteor decay times. *Geophys Res Lett*, 1999, 26(21): 3297-3300.
- 9 Cervera M A, Reid I M. Comparison of atmospheric parameters derived from meteor observations with CIRA. *Radio Sci*, 2000, 35(3): 833-843.
- 10 Hocking W K, Singer W, Bremer J, et al. Meteor radar temperatures at multiple sites derived with SKiYMET radars and compared to OH, rocket and lidar measurements. *J Atmos Sol-Terr Phys*, 2004, 66(6-9): 585-593.
- 11 Holdsworth D A, Morris R J, Murphy D J, et al. Antarctic mesospheric temperature estimation using the Davis mesosphere-stratosphere-troposphere radar. *J Geophys Res*, 2006, 111(D05108), doi: 10.1029/2005JD006589.
- 12 Kumar K K. Temperature profiles in the MLT region using radar-meteor trail decay times: Comparison with TIMED/SABER observations. *Geophys Res Lett*, 2007, 34(L16811), doi: 10.1029/2007GL030704.
- 13 Kim J H, Kim Y H, Lee C-S, et al. Seasonal variation of meteor decay times observed at King Sejong Station (62.22°S, 58.78°W), Antarctica. *J Atmos Sol-Terr Phys*, 2010, 72: 883-889.
- 14 Kim J H, Kim Y H, Jee G, et al. Mesospheric temperature estimation from meteor decay times of weak and strong meteor trails. *J Atmos Sol-Terr Phys*, 2012, 89: 18-26.
- 15 Baumgaertner A J G, McDonald A J. A gravity wave climatology for Antarctica compiled from Challenging Minisatellite Payload/Global Positioning System (CHAMP/GPS) radio occultations. *J Geophys Res*, 2007, 112(D05103), doi: 10.1029/2006JD007504.
- 16 Lee C S, Younger J P, Reid I M, et al. The effect of recombination and attachment on meteor radar diffusion coefficient profiles. *J Geophys Res: Atmos*, 2013, 118(7): 3037-3043.
- 17 Holdsworth D A, Reid I M, Cervera M A. Buckland Park all-sky interferometric meteor radar. *Radio Sci*, 2004, 39(RS5009), doi: 10.1029/2003RS003014.
- 18 Holdsworth D A, Murphy D J, Reid I M, et al. Antarctic meteor observations using the Davis MST and meteor radars. *Adv Space Res*, 2008, 42(1): 143-154.
- 19 Mitchell N J, Beldon C L. Gravity waves in the mesopause region observed by meteor radar: 1. A simple measurement technique. *J Atmos Sol-Terr Phys*, 2009, 71(8-9): 866-874.
- 20 Yoshiki M, Kizu N, Sato K. Energy enhancements of gravity waves in the Antarctic lower stratosphere associated with variations in the polar vortex and tropospheric disturbances. *J Geophys Res*, 2004, 109(D23104), doi: 10.1029/2004JD004870.
- 21 Smith A K. Physics and chemistry of the mesopause region. *J Atmos Sol-Terr Phys*, 2004, 66(10): 839-857.
- 22 Fritts D C, Vadas S L, Wan K, et al. Mean and variable forcing of the

- middle atmosphere by gravity waves. *J Atmos Sol-Terr Phy*, 2006, 68(3-5): 247-265.
- 23 Whiteway J A, Duck T J, Donovan D P, et al. Measurements of gravity wave activity within and around the Arctic stratospheric vortex. *Geophys Res Lett*, 1997, 24(11): 1387-1390.
- 24 Singer W, Latteck R, Millan L F, et al. Radar backscatter from underdense meteors and diffusion rates. *Earth Moon Planet*, 2008, 102(1-4): 403-409.
- 25 Younger J P, Reid I M, Vincent R A, et al. Modeling and observing the effect of aerosols on meteor radar measurements of the atmosphere. *Geophys Res Lett*, 2008, 35(L15812), doi: 10.1029/2008GL033763.
- 26 Ballinger A P, Chilson P B, Palmer R D, et al. On the validity of the ambipolar diffusion assumption in the polar mesopause region. *Ann Geophys*, 2008, 26(11): 3439-3443.
- 27 Friedrich M, Torkar K M, Steiner R J. Empirical recombination rates in the lower ionosphere. *Adv Space Res*, 2004, 34 (9): 1937-1942.
- 28 Hocking W K, Thayaparan T, Franke S J. Method for statistical comparison of geophysical data by multiple instruments which have differing accuracies. *Adv Space Res*, 2001, 27(6-7): 1089-1098.
- 29 Singer W, Bremer J, Hocking W K, et al. Temperature and wind tides around the summer mesopause at middle and arctic latitudes. *Adv Space Res*, 2003, 31(9): 2055-2060.
- 30 Singer W, Bremer J, Weiß J, et al. Meteor radar observations at middle and Arctic latitudes Part 1: mean temperatures. *J Atmos Sol-Terr Phy*, 2004, 66(6-9): 607-616.
- 31 Stober G, Jacobi Ch, Fröhlich K, et al. Meteor radar temperatures over Collm (51.3°N, 13°E). *Adv Space Res*, 2008, 42(7): 1253-1258.
- 32 Alexander M J, Teitelbaum H. Observation and analysis of a large amplitude mountain wave event over the Antarctic peninsula. *J Geophys Res*, 2007, 112(D21103), doi: 10.1029/2006JD008368.